Convection under a lid of finite conductivity in wide aspect ratio models: effect of continents on the wavelength of mantle flow

Cécile Grigné, Stéphane Labrosse, Paul J. Tackley

JOURNAL OF GEOPHYSICAL RESEARCH, VOL. 112, B08403, doi:10.1029/2006JB004297, 2007

Convection under a lid of finite conductivity in wide aspect ratio models: Effect of continents on the wavelength of mantle flow

C. Grigné,[1] S. Labrosse,[2] and P. J. Tackley[1]

Received 18 January 2006; revised 14 February 2007; accepted 18 April 2007; published 1 August 2007.

[1] Mantle convection in the Earth and Mars are dominated by large-scale flow, and this can be due at least in part to the effect of thermally insulating continent-like heterogeneities. Indeed, the presence of a finitely conducting lid on top of a convective isoviscous fluid at infinite Prandtl number induces the formation of a zone of hot upwelling centered beneath the lid and a large horizontal cellular circulation on each side of the lid. In a previous paper, this lateral cellular circulation was limited in size by the dimensions of the model. We now use very large aspect ratio models in order for this circulation to be unhampered. The large-scale circulation consists of the constructive superposition of hot and cold plumes attracted to and expelled from, respectively, the conductive lid. The width of the cellular circulation increases with the Rayleigh number of the fluid, and we propose a scaling law to explain this expansion. Scaling laws for the velocity of the plumes and heat transfer by this large-scale circulation are also developed. Although the model used is much simpler than actual planetary mantles, the driving mechanism for the large-scale circulation must operate in a similar fashion. Important implications in terms of heat transfer can therefore be predicted.

Citation: Grigné, C., S. Labrosse, and P. J. Tackley (2007), Convection under a lid of finite conductivity in wide aspect ratio models: Effect of continents on the wavelength of mantle flow, *J. Geophys. Res.*, *112*, B08403, doi:10.1029/2006JB004297.

1. Introduction

[2] Convection in the mantle of the Earth is dominated by a large-scale circulation, as evidenced by the sizes of plates and the power in the degree 2 of the spherical harmonic expansions of the gravity field and tomographic models [*Hager et al.*, 1985; *Su and Dziewonski*, 1991; *Woodward and Masters*, 1991; *Zhang and Tanimoto*, 1991; *Montagner*, 1994]. This observation is at odds with the dynamics of standard Rayleigh Bénard convection in which the typical horizontal wavelength of circulation is about twice the depth of the convective layer [e.g., *Koschmieder*, 1993], that is convective cells of aspect ratio 1. In the physics literature, a transition to large-scale flow at high Rayleigh number has been observed [*Krishnamurti and Howard*, 1981] but this has been attributed to the Reynolds stress due to plumes, which is nonexistent at infinite Prandtl number, the regime that is relevant to planetary mantles. Other solutions have been proposed to generate this large-scale flow, like depth-dependent physical properties [e.g., *Hansen et al.*, 1993; *Tackley*, 1996; *Dubuffet et al.*, 1999; *Busse et al.*, 2006] and the effects of continents [e.g., *Gurnis*, 1988; *Zhong and Gurnis*, 1993; *Yoshida et al.*, 1999; *Honda et al.*, 2000; *Phillips and Bunge*, 2005]. This last effect is the one investigated in the present paper.

[3] A fixed lid of finite thermal conductivity set on top of an isoviscous fluid of infinite Prandtl number induces the formation of a zone of hot upwelling centered beneath this lid, which feeds a horizontal cellular circulation on each side of the lid [e.g., *Guillou and Jaupart*, 1995; *Lenardic and Moresi*, 2001; *Grigné et al.*, 2007]. The zone of hot upwelling can consist of either one fixed plume, for low Rayleigh numbers, or of a set of small plumes, at high Rayleigh number. At high Rayleigh number the convection is time-dependent and hot plumes, forming at the bottom boundary layer of the model away from the lid, are attracted toward the center of the lid, while cold plumes are expelled from the lid. A time averaging method is used to study the lateral extent of the circulation induced by the lid, and we observe that this circulation is wider at higher Rayleigh numbers.

[4] The effect of the horizontal scale of flow on heat transfer has been the subject of several studies [e.g., *Olson and Corcos*, 1980; *Hansen and Ebel*, 1984; *Turcotte and Schubert*, 1982, 2002; *Grigné et al.*, 2005] and it was generally found that the heat flow dependence on the wavelength is maximum for cells that are approximately square. Consequently, continents would affect the thermal evolution of the Earth not only by reducing the effective surface of cooling [*Grigné and Labrosse*, 2001], but also by changing the wavelength of mantle convection. In addition to quantifying the effect of a conductive lid on the wave-

[1] Institut für Geophysik, ETH Zürich, ETH Hönggerberg HPP, Zürich, Switzerland.
[2] Sciences de la Terre, Ecole Normale Supérieure de Lyon, Lyon, France.

0148-0227/07/2006JB004297$09.00

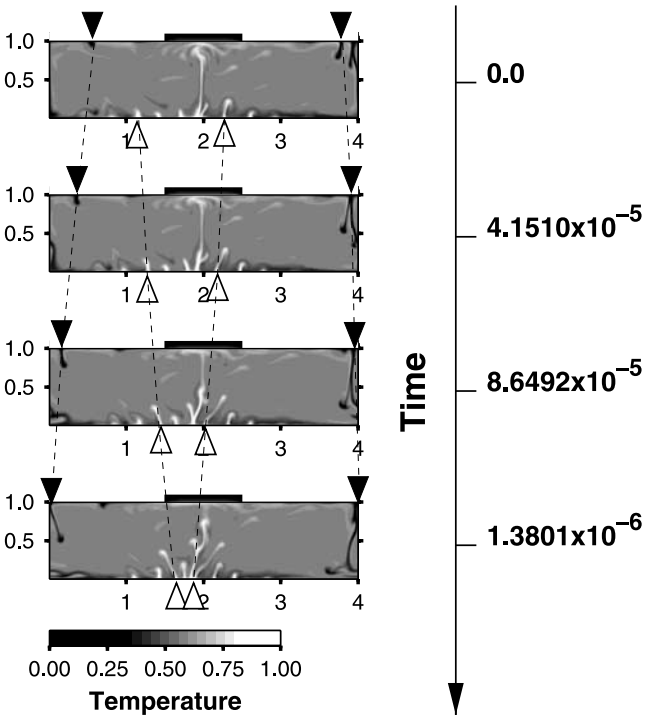

Figure 1. Snapshots of the temperature field obtained at $Ra = 10^7$ under a lid of width $a = 1$ and Biot number $B = 10$, at different times, taking $t = 0$ at an arbitrary instant (top). The open triangles follow hot plumes attracted toward the center of the lid, while black triangles follow cold plumes in the upper boundary layer.

length of convection, we study the implications it has in terms of heat transfer.

[5] The pattern of convection obtained for two-dimensional experiments carried out in wide aspect ratio boxes is presented in section 2 and is compared to what is obtained when the model has an aspect ratio equal to or smaller than 4. In section 3, a scaling law is proposed to explain why the size of the cellular circulation generated by the lid increases with the Rayleigh number. In section 4 we present a scaling law for the heat transfer in wide aspect ratio boxes. The implications of the observed thermal features in our experiments for the Earth's mantle are discussed in section 5.

2. Model and Phenomenology

2.1. Model: Boundary Conditions

[6] The experiments we carry out in the present paper are similar to the ones presented in *Grigné et al.* [2007]: we use two-dimensional Cartesian models and solve the equations of convection for an isoviscous fluid at infinite Prandtl number, using the code Stag written by P. Tackley [e.g., *Tackley*, 1993]. We use a regular grid with square cells, with 64 cells in the vertical direction at Rayleigh numbers less than or equal to 10^6, and 128 cells for larger Rayleigh numbers. Numerical experiments are continued until a statistical stationary state is reached, that is to say until the time evolution of temperature and heat flux in the model involves only fluctuations around a mean value. All the examples of temperature and velocity fields presented hereafter are obtained in this statistical stationary state. We explicitly choose to use free-slip boundary conditions at the bottom and at the top of the fluid, with no mechanical coupling between the lid and the fluid, in order to study the thermal effect of the lid on the fluid in an isolated way. Periodic boundary conditions are used on the vertical walls of the model.

[7] The fluid is heated from below, and a condition of fixed temperature is imposed at the bottom of the model. At the surface, thermal conditions of mixed-type [*Sparrow et al.*, 1964; *Grigné et al.*, 2007] are imposed: a finitely conducting lid is put on top of the model, partially covering its surface. A fixed zero temperature is imposed at the surface of the fluid outside of the lid. At the interface between the lid and the fluid, continuity of temperature and heat flux is imposed. A zero temperature is then applied at the surface of the lid and on its vertical boundaries.

[8] The thermal condition at the surface of the fluid located under the lid is of mixed type. It can be described by a dimensionless number, called Biot number B [*Sparrow et al.*, 1964]:

$$B = \frac{k_c}{k}\frac{d}{d_c}, \tag{1}$$

where k_c and k are the thermal conductivities of the lid and of the fluid, respectively, and d_c and d are their respective thicknesses. This number describes the insulating effect of the lid [see *Sparrow et al.*, 1964; *Guillou and Jaupart*, 1995; *Grigné et al.*, 2007]: If the lid is very thick ($d_c \to \infty$) or with a low conductivity ($k_c \to 0$), then the lid is very insulating ($B \to 0$), and the boundary condition at its base tends toward one of fixed zero heat flux. On the other hand, a thin ($d_c \to 0$) or very conductive ($k_c \to \infty$) lid implies a thermal boundary condition close to one of fixed temperature ($B \to \infty$).

[9] We use the following parameters to render the system of equations nondimensional: The characteristic length is the depth of the mantle d, the characteristic temperature is the superadiabatic temperature jump ΔT across the mantle, and the characteristic time and velocity are $[t] = d^2/\kappa$ and $[u] = \kappa/d$, respectively, where κ is the thermal diffusivity of the mantle. The Rayleigh number is

$$Ra = \frac{\rho\alpha g \Delta T d^3}{\kappa\mu}, \tag{2}$$

where ρ, α and μ are the reference density, thermal expansion and dynamic viscosity of the mantle, respectively. In the remainder of this paper, the asterisk is added to parameters that are made dimensionless.

2.2. Phenomenology

[10] Snapshots of the temperature fields obtained with such models, with a lid of Biot number $B = 10$ and of nondimensional width $a = 1$, at a Rayleigh number $Ra = 10^7$, in a model of aspect ratio 4, are presented in Figure 1. We choose a lid of Biot number $B = 10$ because this value corresponds to the Biot number of the continental lithosphere for whole mantle convection: If the thermal conductivity of the continental lithosphere is considered to be the same as the one of the mantle, then this Biot number $B = 10$

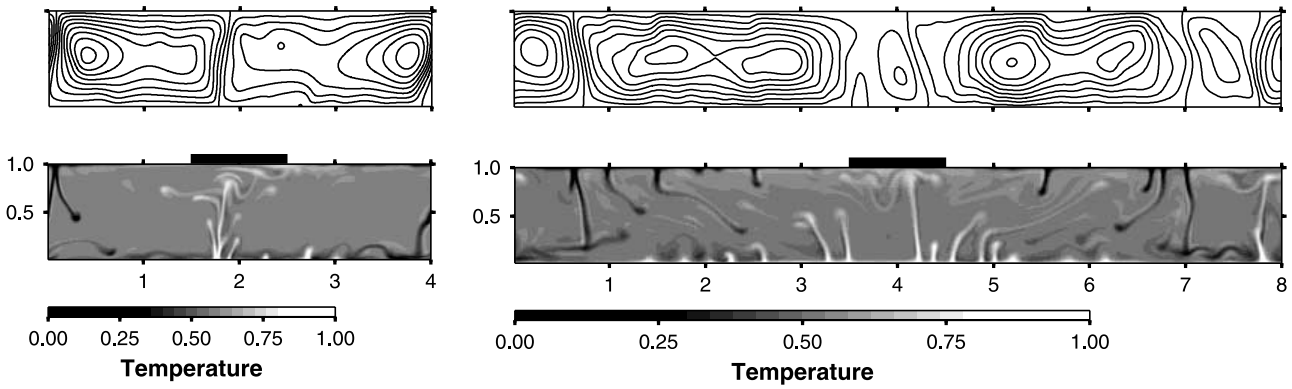

Figure 2. Snapshots of (top) the streamlines and (bottom) temperature fields obtained at $Ra = 10^7$, for a continental lid of Biot number $B = 10$ and of dimensionless width $a = 1$, for models of aspect ratio (left) 4 and (right) 8.

corresponds to a continental lithosphere thickness equal to one tenth of that of the mantle, that is to say close to 300 km, which is within the estimates obtained by heat flux measurements [e.g., *Rudnick et al.*, 1998; *Jaupart and Mareschal*, 1999; *Michaut and Jaupart*, 2004].

[11] A set of hot plumes is clearly present beneath the lid (Figure 1). Different time steps are shown in Figure 1 and indicate that these hot plumes in the bottom boundary layer are attracted toward the center of the model, while cold plumes forming in the upper boundary layer are expelled toward the vertical boundaries of the model. The temperature field and the stream function of the flow for this case are presented in Figure 2, as well as a model of aspect ratio 8 with the same lid and Rayleigh number. In the model of aspect ratio 8 (Figure 2, right), a zone of upwelling, consisting of a set of hot plumes, is also present under the lid. The presence of two convective cells is visible in the snapshot of the streamlines. It also appears that these convective cells are not spread out over the whole half width of the model, in contrast to the model of aspect ratio 4. In this latter case, a simple loop model is a good approach to understand the scaling of the heat transfer and of the velocity in the model [e.g., *Turcotte and Schubert*, 1982, 2002; *Grigné et al.*, 2005]. For the model of width 8, the flow is more complex, and the scaling law proposed by *Grigné et al.* [2007] for the heat flux does not apply straightforwardly.

[12] Figure 2 (right) shows that the lateral circulation generated by the presence of the lid is wide. In order to study the maximum extent of this lateral circulation, we use models of aspect ratio 32, with a lid of width $a = 1$. Snapshots of the temperature fields and of the streamlines are presented in Figure 3 for Rayleigh numbers varying from 10^5 to 10^8. At $Ra = 10^5$, convective cells are clearly visible in both the temperature field and the streamlines. The cells with the hot upwelling located under the lid, which we will call, for simplicity, "continental cell" in the remainder of this paper, have a dimensionless width $L \simeq 2.5$, while the other cells in the models have an aspect ratio $L = 1.7 \pm 0.2$. At $Ra = 10^6$, the continental cell has a width close to 3. Cells outside of the lid have a normal aspect ratio, between 1 and 1.7.

[13] At higher Rayleigh numbers, no clear convective cell can be detected in the snapshots of the temperature fields, but it remains clear from the streamlines of the flow that a large-scale circulation is present, in contrast to normal cells visible far away from the lid. In the examples with $Ra = 10^7$ and $Ra = 10^8$, convection is highly time-dependent, with small hot plumes forming far away from the lid and attracted toward it, while cold plumes are expelled from the lid. An important feature of Figure 3 is that the width of the continental cells clearly increases with the Rayleigh number. In order to compare the mean behavior of the flow for the different Rayleigh numbers, we compute the time-averaged temperature, velocity and stream function fields. Time-averaged streamlines are, for instance, presented in Figure 4.

3. Width of the Cellular Circulation

3.1. Time-Averaged Circulation

[14] Figure 4 presents the time-averaged stream function for the cases $Ra = 10^7$ and $Ra = 10^8$ with a lid of Biot number $B = 10$ and of width 1. Figure 4 explains how we compute the width of the cellular circulation generated by the lid. The positions x_0 and x_1 denote the limits of this circulation: x_0 is the position of the center of the lid ($x_0 = 16$ in Figure 4), and x_1 is the position where the time-averaged stream function at middepth changes sign. $\overline{\Lambda}$ denotes the convective cell width derived this way from the time-averaged stream function.

[15] Figure 5 represents the values of $\overline{\Lambda}$ as a function of the Rayleigh number for experiments carried out in boxes of width 32, with a lid of width 1 and of Biot number $B = 10$. Instantaneous values of Λ can be obtained from snapshot of the stream function, and the error bars in Figure 5 are computed as the standard deviation between the time-averaged value $\overline{\Lambda}$ and instantaneous values of Λ. Figure 5 shows that the width $\overline{\Lambda}$ scales as $Ra^{1/4}$. An explanation for this scaling is derived in two steps: We first consider the hot zone under the lid and study the velocity of the plumes in that zone. In the second step, we consider the driving force for the horizontal circulation.

3.2. Vertical Velocity Scaling

[16] *Grigné et al.* [2007] defined two regimes of cellular circulation generated by the lid, which depend on the geometry of the model and of the lid, and on the Rayleigh

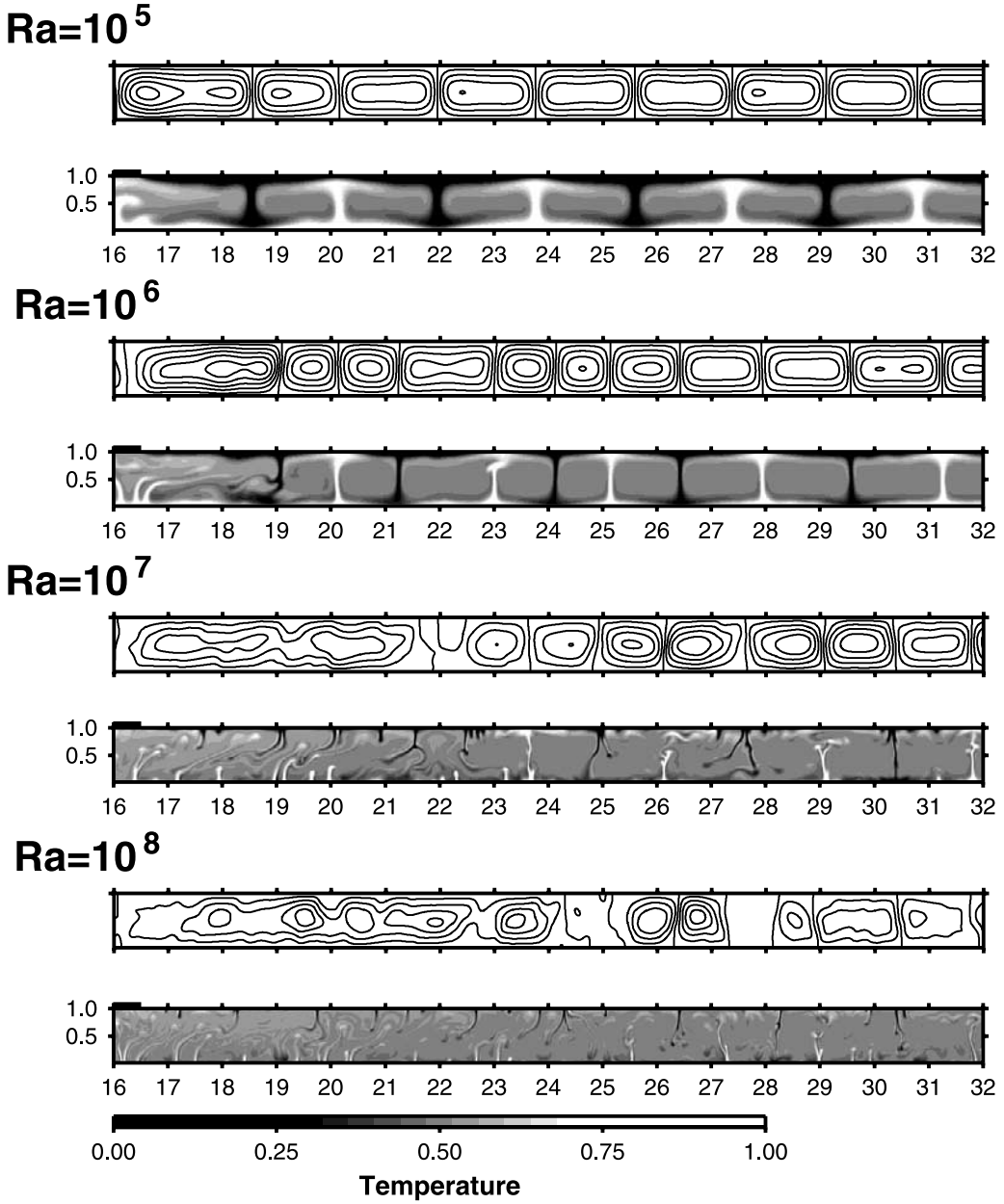

Figure 3. Snapshots of the temperature field and of the stream function obtained in models of aspect ratio 32, for a lid of width 1 and Biot number $B = 10$, for different Rayleigh numbers. Only the right half of the model is shown, the flow being statistically symmetrical compared to the center of the lid. The same shading scale is used for the different Rayleigh numbers.

number. For low Rayleigh numbers or large lids, the circulation is steady state or weakly time-dependent, and can be described as a perfect convective cell, with a single hot plume under the lid and a single cold plume along the vertical boundaries of the model. This regime was named "forced loop" because the geometry of the model is such that cold and hot plumes do not develop freely by destabilization of the boundary layers, but their position is forced by the size of the model. For narrower lids or larger boxes, when the Rayleigh number is large enough ($Ra \geq 10^6$) the zone of upwelling under the lid is not formed by a single plume but by a set of hot plumes attracted toward the center of the model. We named that regime "free loop." In that case, the time-averaged vertical velocity at middepth is smaller in amplitude than the one along the vertical downwelling, which is opposite to simple Rayleigh-Bénard convection or to the forced loop case, where the velocity of the hot and cold plumes are the same.

[17] For wide aspect ratio models and for $Ra > 10^5$ the regime is clearly one of free loop, with a zone of upwelling under the lid formed by several hot plumes. Figure 6 presents the time-averaged vertical velocity at middepth under the lid as a function of the Rayleigh number, as well as the vertical velocity of plumes located far away from the lid. These two velocities are denoted by W_h and W, respectively, in Figure 6. For simple Rayleigh-Bénard convection,

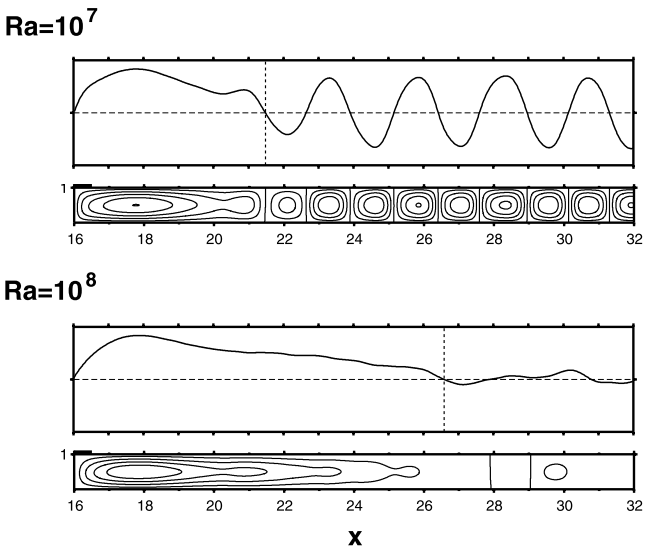

Figure 4. Time-averaged stream function for the experiments presented in Figure 3 with $Ra = 10^7$ and 10^8 and its profile at middepth. The vertical dashed line indicates the position x_1 where the stream function changes sign. As in Figure 3, only the right half of the model is presented.

the time-averaged vertical velocity of plumes and the horizontal velocity along the horizontal boundaries of the model both scale as $Ra^{2/3}$ [e.g., *Turcotte and Schubert*, 1982, 2002; *Grigné et al.*, 2005]. Here, the vertical velocity under the lid W_h clearly scales as $Ra^{1/2}$.

[18] This can be explained by studying the form of the convective heat flux under the lid. This convective heat flux at a depth z is

$$A(z) = \rho C_p v_z \left(T - \overline{T(z)}\right), \tag{3}$$

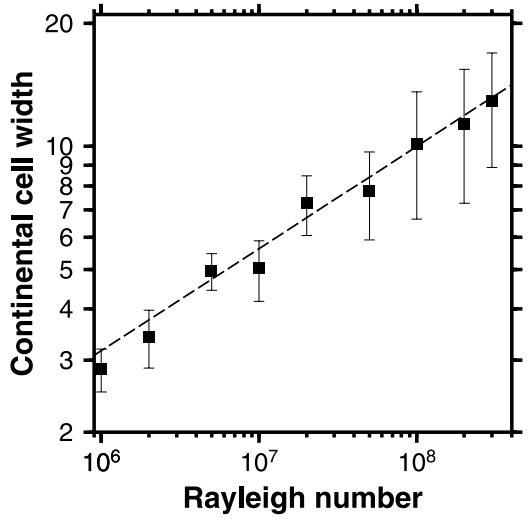

Figure 5. Width $\overline{\Lambda}$ of the continental cell, as defined in section 2.2, as a function of the Rayleigh number, for a lid of width 1 and Biot number $B = 10$, for models of aspect ratio 32. Error bars represent the standard deviation between instantaneous values of Λ and the time-averaged value $\overline{\Lambda}$. The dashed line is drawn using $\overline{\Lambda} = 0.1\ Ra^{1/4}$.

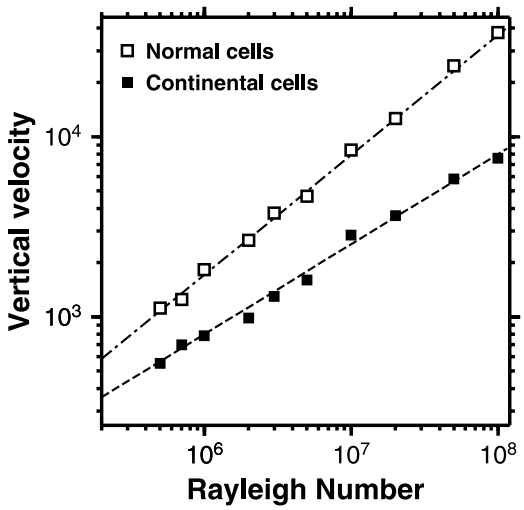

Figure 6. Time-averaged vertical velocity as a function of the Rayleigh number for experiments with a lid of width 1 and Biot number $B = 10$. Solid squares are for the vertical velocity at middepth under the center of the lid (continental cell), and open squares are for the plumes far away from the lid (normal convective cells). The dash-dotted and dashed lines are drawn using $W = 0.17\ Ra^{2/3}$ and $W_h = 0.8\ Ra^{1/2}$, respectively.

where C_p is the heat capacity of the fluid, v_z the vertical velocity and $\overline{T(z)}$ is the horizontally averaged temperature at the depth z. The dimensionless form of the convective heat flux is

$$A^* = v_z^* \left(T^* - \overline{T^*(z)}\right). \tag{4}$$

Figure 7 presents this time-averaged convective heat flux for a model of aspect ratio 4, with a Rayleigh number $Ra = 10^7$, for a lid of Biot number 10 and of width 1 and 2,

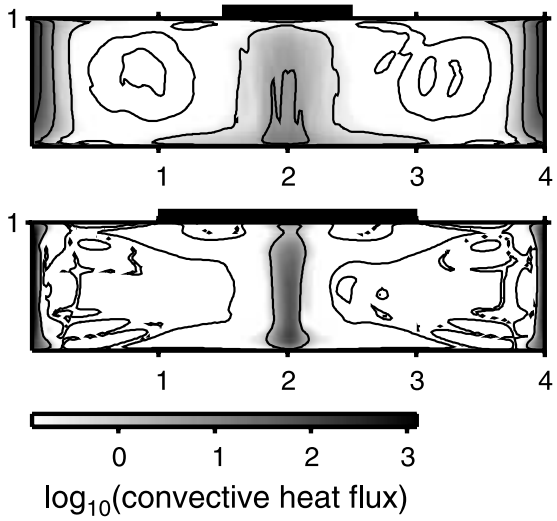

Figure 7. Contour lines of the time-averaged convective heat flux (equation (3)) for $Ra = 10^7$ with a model of aspect ratio 4. The continental lid has a Biot number $B = 10$, and a width (top) 1 or (bottom) 2.

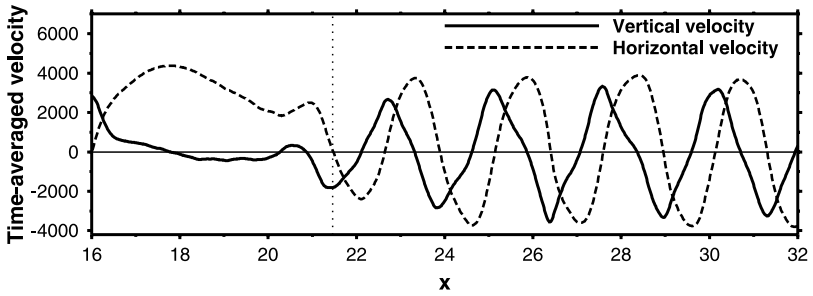

Figure 8. Horizontal profiles of the time-averaged vertical velocity at middepth and horizontal velocity at the surface of the model for a model of aspect ratio 32, at $Ra = 10^7$, with a lid of width 1 with $B = 10$. Only the right half of the model is presented. The center of the lid is located at $x = 16$. The vertical dotted line shows the limit of the cellular circulation generated by the lid, as computed in Figure 4.

which yields a free loop and a forced loop regime, respectively. For the latter regime, there is symmetry between the cold and hot plumes, and the zone of nonnegligible convective heat flux is restricted to narrow zones whose width is of the same order as that of the thermal plumes. This width where the convective heat flux is nonzero then scales as $Ra^{-1/3}$ [e.g., *Turcotte and Schubert*, 1982, 2002; *Grigné et al.*, 2005]. For the free loop regime, heat is carried under the lid not by one plume, but by a set of hot plumes attracted toward the center of the model. This creates a zone of nonzero convective heat flux which spreads over the whole region where the vertical velocity is nonzero. The width of this zone, denoted by λ hereafter, depends weakly on the Rayleigh number and is of the order of the half depth of the model [*Grigné et al.*, 2005].

[19] For the free loop regime, the total convective heat flow for the hot zone under the lid is then

$$A_h \sim \rho C_p W_h \lambda (T_h - T_m), \tag{5}$$

where W_h is the time-averaged vertical velocity at middepth under the lid, T_h the mean temperature under the lid and T_m the temperature in the well-mixed center of the convective cell. The temperature anomaly $(T_h - T_m)$ is responsible for the buoyancy force of each plume beneath the lid, denoted by F_h, which reads

$$F_h \sim \rho \alpha g \delta (T_h - T_m), \tag{6}$$

where α is the coefficient of thermal expansion, g is the gravitational acceleration, and δ is the width of each individual plume. It is to be noted that the width λ of the region of nonzero convective heat flux is different from the width δ of individual plumes, precisely because this region is made up of the sum of contributions from all plumes. This is opposite to what would be obtained in a classical loop model of a convective cell, where the widths to consider for the convective heat flux and for the buoyancy force are the same.

[20] The temperature anomaly $(T_h - T_m)$ can be eliminated from equations (5) and (6) to give

$$W_h F_h \sim \frac{\alpha g}{C_p} \frac{\delta}{\lambda} A_h, \tag{7}$$

which is the scaling for the power of the buoyancy force. We then write the equilibrium between the buoyancy force and the viscous drag $\tau = \mu \, \partial_x w$, where μ is the dynamic viscosity of the fluid. We previously showed [*Grigné et al.*, 2005] that the horizontal profile of vertical velocity was such that $\partial_x w \sim W_h/\lambda$. With equation (7), the equilibrium between the work of the buoyancy force and that of the viscous drag ($W_h F_h \sim \mu W_h^2/\lambda$) gives

$$W_h^2 \sim \frac{\alpha g \lambda}{\mu C_p} \frac{\delta}{\lambda} A_h, \tag{8}$$

which, in a dimensionless form, reads

$$W_h^{*2} \sim Ra \; \delta^* \; A_h^*. \tag{9}$$

The convective heat flow A_h^* is responsible for the heat flow out of the model, which is inversely proportional to the thickness of the horizontal boundary layer, which is itself proportional to the width δ of the individual plumes, yielding $A_h^* \sim 1/\delta^*$. We thus obtain

$$W_h^* \sim Ra^{1/2}. \tag{10}$$

[21] The fact that the time-averaged convective heat flux is nonzero over a finite width larger than the width of the individual plumes, due to the pattern of convection consisting of a set of hot plumes moving toward the center of the lid, thus leads to a vertical velocity that scales as $Ra^{1/2}$, and not $Ra^{2/3}$ as is obtained for simple Rayleigh-Bénard convection, where heat is carried out by single cold and hot plumes that consequently have to move faster (see Figure 6).

3.3. Width of the Cellular Circulation and Velocity of Plumes

[22] The driving force for the large horizontal circulation generated by the lid is the horizontal thermal gradient that exists between the abnormally hot zone under the continental lid and the normal fluid far from the lid. This cellular circulation takes place in the form of cold small plumes expelled far from the lid at the top of the model, and hot plumes attracted toward the center of the box at the base of the model. The upwelling zone is concentrated under the lid because of the convergence of hot plumes coming from both sides, while the downwelling takes place in a broader zone since the width of the domain is larger than the intrinsic size of the large-scale circulation. This flow pattern can be seen in Figure 8: The vertical velocity at middepth

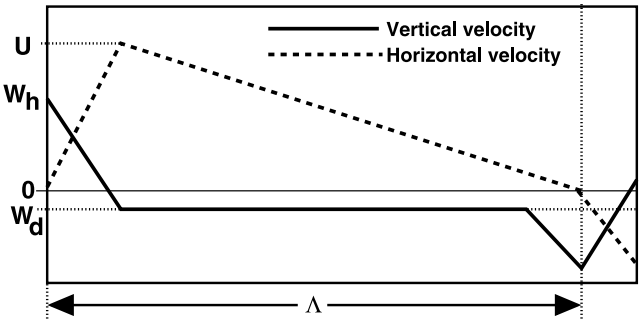

Figure 9. Model used in this study for the time-averaged vertical velocity at middepth and for the horizontal velocity at the surface.

peaks under the lid at $x = 16$ and is close to zero over a large width, where the cellular circulation takes place. It should, however, be noted that the cold plumes carry a nonnegligible amount of mass downward, and the vertical velocity is slightly negative in this zone. This feature is more clearly visible in the profile of the horizontal velocity at the surface also presented in Figure 8: This velocity decreases almost linearly from the edge of the lid to the border of the continental cell. To achieve mass conservation, it is then required that the vertical velocity at middepth in the center of the cellular circulation is negative. We call W_d this small vertical negative velocity created by the descending cold plumes. The model and the notations that we use for the horizontal velocity profiles are presented in Figure 9.

[23] U denotes the maximum horizontal velocity, as indicated in Figure 9. Mass conservation implies

$$W_d/d \sim U/\Lambda. \tag{11}$$

It also implies $U/\lambda \sim W_h/d$, which yields $U^* \sim Ra^{1/2}$ with equation (10). The velocity U is plotted in Figure 10, showing the scaling $U^* \sim Ra^{1/2}$. $\Delta_h T$ denotes the temperature difference between the center of the model, under the lid, and the normal fluid, starting at the position $x = \Lambda$. The buoyancy force created by the horizontal thermal gradient is

$$F \sim \rho g \alpha \, \Lambda \, \Delta_h T. \tag{12}$$

Figure 11 presents the horizontal profiles of time-averaged temperature at middepth for different Rayleigh numbers. The anomaly is spread more widely at higher Rayleigh numbers, but its amplitude is smaller. In dimensionless form, $\Lambda^* \Delta_h T^*$ does not appear to depend on the Rayleigh number to first order. Observing that $\Lambda^* \sim Ra^{1/4}$, this implies $\Delta_h T \sim Ra^{-1/4}$. This scaling is indeed observed, as shown in Figure 12.

[24] The force opposing the horizontal circulation is mostly the horizontal viscous shear stress applying on the width Λ: $\tau \sim \mu \, U/d$. The equilibrium between the work of the buoyancy force F and that of the viscous shear stress integrated on the loop is then

$$W_d F d \sim \mu \frac{U^2}{d} \, \Lambda. \tag{13}$$

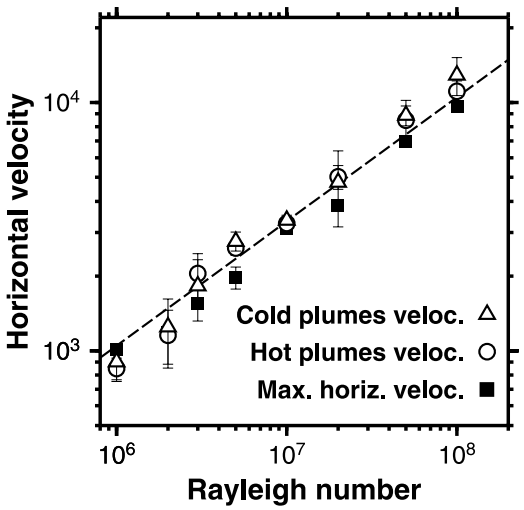

Figure 10. Maximum horizontal velocity U^* at the surface of models with a lid of width $a = 1$ and Biot number $B = 10$ (black squares) and time-averaged horizontal velocity of cold plumes expelled from the lid (open triangles) and of hot plumes attracted toward the center of the lid (open circles). The dashed line is drawn using $U^* = 1.05 \, Ra^{1/2}$.

With equations (11) and (12), this leads to

$$\rho g \alpha (\Lambda \Delta_h T) d^3 \sim \mu U \, \Lambda^2, \tag{14}$$

or, in dimensionless form:

$$Ra(\Lambda^* \Delta_h T^*) \sim U^* \, \Lambda^{*2}. \tag{15}$$

Noting that $(\Lambda^* \Delta_h T^*)$ does not depend on Ra and that $U^* \sim Ra^{1/2}$, we finally obtain for the width Λ^* in a dimensionless form:

$$\Lambda^* \sim Ra^{1/4}. \tag{16}$$

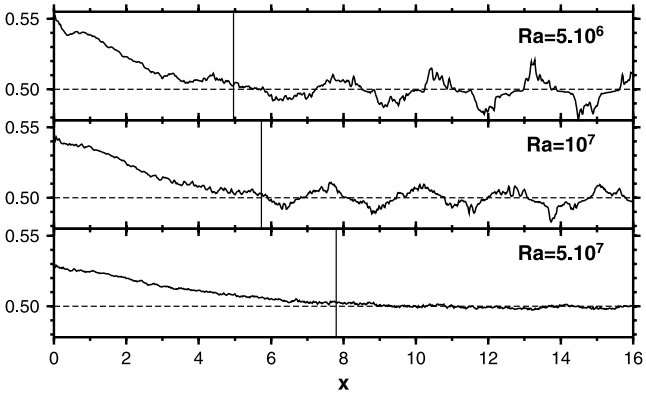

Figure 11. Time-averaged temperature at middepth of the model at different Rayleigh numbers, presented for the right half of the model. The center of the lid is at $x = 16$, and the lid is of width 1 and Biot number 10. The vertical lines represent the limit of the continental cell, as defined in section 2.2.

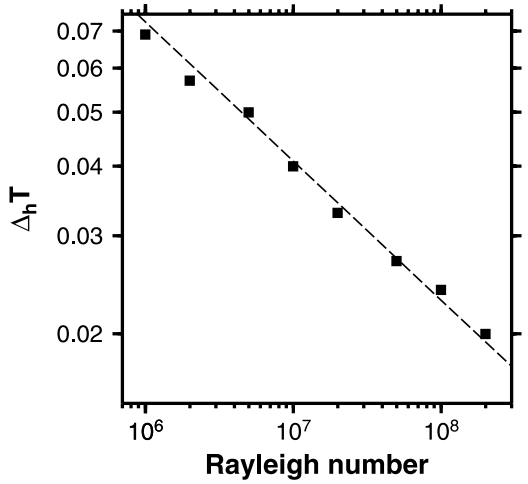

Figure 12. Time-averaged difference of temperature $\Delta_h T = T_c - T_m$ as a function of Ra, where T_c is the temperature below the center of the lid (position $x = 0$ in Figure 11) and $T_m = 0.5$. The dashed line is drawn using $\Delta_h T = 2.30\, Ra^{-1/4}$.

The scaling law $\Lambda^* = 0.1\, Ra^{1/4}$ is plotted in Figure 5, and fits well the observed widths Λ. The derivation of this scaling law did not take into account the size of the lid a. The purpose here was to understand the dependency of Λ^* on Ra and we used a small lid whose size can be neglected compared to the size of the cellular circulation. However, the latter also depends on the size of the lid, and for the case of a strongly insulating lid, that is to say when it can be considered that the cooling of the upper thermal boundary layer effectively starts only after the edge of the lid, a good empirical scaling is $\Lambda^* = 0.1\, Ra^{1/4} + a^*/2$.

[25] As mentioned above, the large horizontal circulation takes place in the form of cold plumes expelled from the lid and hot plumes attracted toward the center of the continental lid (see Figures 1 and 3). The positions of the plumes can be detected at each time step, using for instance a measurement of the boundary layer Rayleigh number Ra_δ. The heat flux at the surface of the model can be written [*Howard*, 1964; *Sotin and Labrosse*, 1999]

$$q = \left(\frac{Ra}{Ra_\delta}\right)^{1/3} (T_m - T_0)^{4/3}. \tag{17}$$

Knowing the distribution of the heat flux at the surface of the model, we can compute Ra_δ, which peaks above starting cold downwellings. An example of the observed form of this boundary layer Rayleigh number Ra_δ at the surface of the model is presented in Figure 13. The same method can be applied at the base of the model to detect hot upwellings. The positions of the plumes are then defined using a threshold Ra_c for Ra_δ. Different values of Ra_c were used, and we observed that the choice of Ra_c within the range $30 < Ra_c < 500$ does not significantly influence the results, since Ra_δ clearly peaks above cold plumes. We are then able to follow the position of plumes over time and to derive their horizontal velocity. Figure 10 presents the obtained velocities as a function of Ra for experiments carried out with a lid of width $a = 1$ and Biot number $B = 10$. It shows that the plumes are transported by the large horizontal circulation and have broadly the same velocity as the one observed along the horizontal boundaries of the model, scaling as $Ra^{1/2}$.

4. Heat Flux Scaling

[26] *Grigné et al.* [2007] proposed the following scaling law, in dimensionless form, for the heat flux out of a convective cell partially covered by a perfectly insulating lid:

$$Q = \left(\frac{2}{\pi}\right)^{2/3} \frac{Ra^{1/3} T_m^{4/3}}{\left(L^2 + \frac{L}{8\lambda^3}\right)^{1/3}} \left(1 - \frac{a}{2L}\right)^{1/2}, \tag{18}$$

where T_m is the mean temperature of the fluid obtained for simple Rayleigh-Bénard convection, that is to say $T_m = 0.5$, and L is the width of the convective cell. The asterisk is now dropped for the sake of simplicity and all the parameters are now dimensionless in the remainder of this paper. For models of moderate aspect ratio, L is the half width of the model. We showed that the agreement between this scaling law and the observed heat flux was good for models with an aspect ratio up to 4, that is to say convective cells not larger than 2.

[27] However, if we apply this scaling law directly to models in wide aspect ratio boxes, using for the width L of the convective cells the width Λ of the cellular circulation generated by the lid as defined in section 3.1, the heat flux predicted by the model given by equation (18) is always too low. The model given by equation (18) indicates a significant decrease of the heat flux with the size L of the convective cells: For a given Rayleigh number and a fixed size $a = 1$ of the lid, the predicted heat flux is for instance

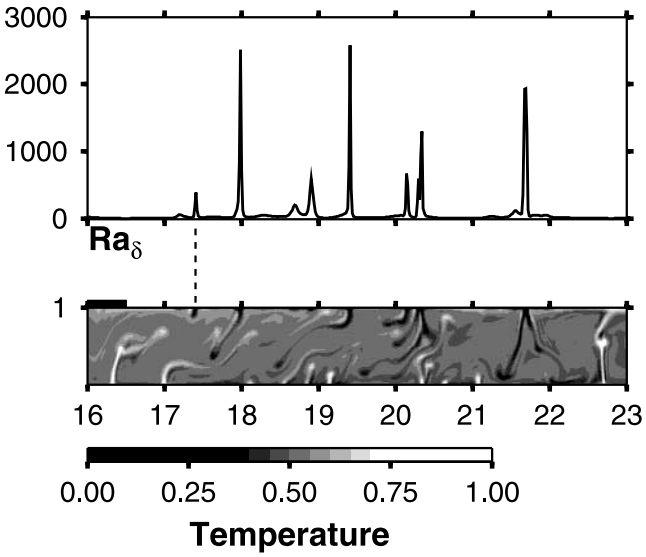

Figure 13. Close up on a part of the temperature field obtained at $Ra = 10^7$ under a perfectly insulating lid of width $a = 1$, with its center at $x = 16$, and the corresponding upper boundary layer Rayleigh number Ra_δ. The vertical dashed line indicates the position of the first detected cold downwelling after the edge of the lid.

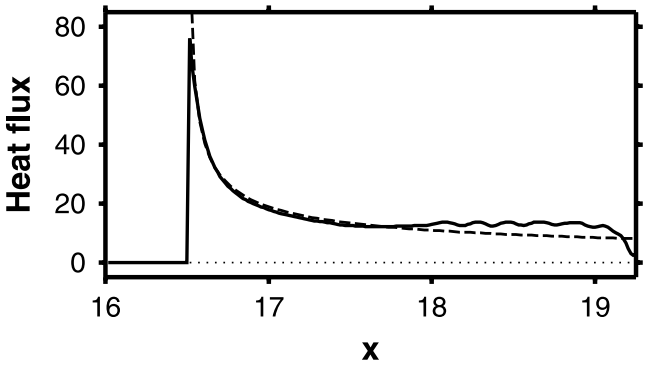

Figure 14. Observed time-averaged heat flux at the surface of a model with a perfectly insulating lid of width $a = 1$, with $Ra = 10^6$ (solid line), and heat flux given by the model of cooling by conduction in a half-space (dashed line), considering that the thermal boundary layer starts to cool and thicken at the edge of the lid.

almost 50% lower for a cell of width $L = 8$ than for a cell of width $L = 4$. The observed heat flux in these two cases actually differ only by around 10%.

[28] Snapshots of the temperature fields obtained in wide aspect ratio boxes show that the circulation generated by the lid is not a simple convective cell, but consists of a set of hot plumes under the lid and cold plumes forming in the top boundary layer and being pushed away from the lid (see Figures 2 and 3). The model proposed by *Grigné et al.* [2007] uses the assumption that the flow can be described by a simple loop model [e.g., *Turcotte and Schubert*, 1982, 2002; *Grigné et al.*, 2005] and that the heat flux at the surface of the convective cells is, to first order, well approximated by a model of cooling by conduction on a half-space, with a heat flux decreasing away from the edge of the lid due to the cooling and thickening of the upper boundary layer.

[29] This assumption does not hold anymore for wide aspect ratio models. Figure 14 presents the observed heat flux obtained in a model of aspect ratio 32, with a perfectly insulating lid of width 1 at $Ra = 10^6$. After some distance from the edge of the lid, the observed heat flux clearly differs from the half-space cooling model presented with a dashed line, which corresponds to the following equation in dimensionless form [see *Grigné et al.*, 2007]:

$$q_h(x) = \frac{Ra^{1/3}(T_m - T_0)^{4/3}}{(2\pi^2)^{1/3}\left(h^2 + \frac{h}{8\lambda^3}\right)^{1/3}}\left(\frac{h}{x - \frac{a}{2}}\right)^{1/2}, \qquad (19)$$

where λ, the width over which the vertical velocity is nonnegligible, is observed to be close to the depth of the model, or in dimensionless form $\lambda = 1$ (whereas $\lambda = 0.5$ in small aspect ratio domains [*Grigné et al.*, 2005]). h is the distance at which the heat flux deviates from this expression. This model is obtained by considering that the thermal boundary layer starts to thicken after the edge of the lid, located at $x = a/2$. The reason for the deviation after $x = h$ is the destabilization of the boundary layer and the onset of cold plumes. The heat flux for $x > h$ then stays broadly constant.

[30] This observation is similar to the familiar flattening of the sea floor after ages larger than 80 Myr (see *Jaupart et al.* [2007] for a review) except that, here, the whole boundary layer is destabilized instead of the small active boundary layer that exists under a stagnant lid caused by temperature-dependent viscosity [e.g., *Davaille and Jaupart*, 1994]. We can then rely on the same approach as that used for computing the total heat loss of the Earth [*Jaupart et al.*, 2007]: We use the half-space cooling equation (19)) for $x < h$ and a uniform heat flux for $x > h$ (Figure 15). The heat flux for $x > h$ is not strictly uniform and small fluctuations

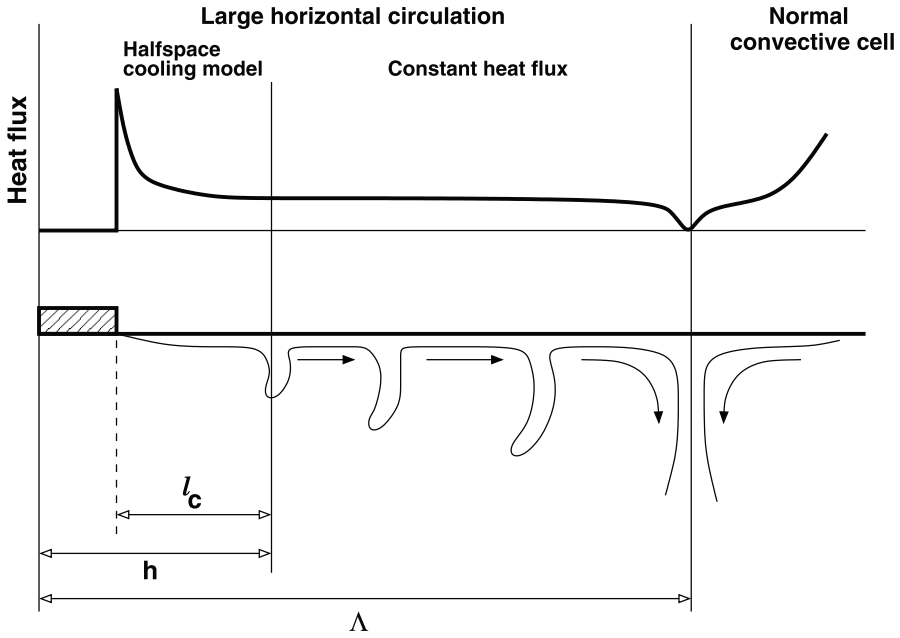

Figure 15. Scheme of the model used to compute the mean heat flux over the large-scale circulation of width Λ generated by the lid.

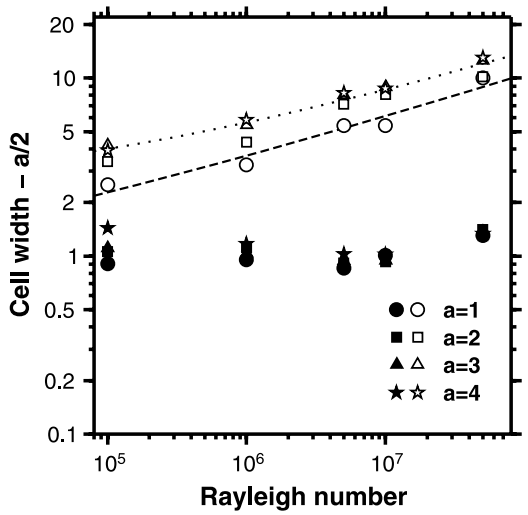

Figure 16. Size of the cellular circulation Λ minus the half width of the lid, obtained with perfectly insulating lids of variable width, as indicated by the symbols, as a function of the Rayleigh number. The open symbols are values obtained using the criteria on the time-averaged stream function described in section 3.1, while the solid symbols are the lengths ℓ_c that give the observed heat flux with the heat flux scaling given by equation (21). The dashed and dotted lines are plotted using $\Lambda = 0.1\ Ra^{1/4} + a/2$, with $a = 1$ and $a = 4$, respectively.

seen on Figure 14 are caused by the different plumes. However, the averaged value is set by the stability of the boundary layer and is equal to the standard value without a lid.

[31] The mean heat flux $\overline{Q}$ over the cellular circulation of width Λ can then be computed using

$$\Lambda\ \overline{Q} = \int_{x=a/2}^{h} q_h(x)\ dx + (\Lambda - h) q_h(x = h). \qquad (20)$$

With equation (19), this yields

$$\overline{Q} = \left(\frac{2}{\pi}\right)^{2/3} \frac{Ra^{1/3}(T_m - T_0)^{4/3}}{2\Lambda\left(h^2 + \frac{h}{8\lambda^3}\right)^{1/3}} \left(\frac{h}{h - a/2}\right)^{1/2} (\Lambda + h - a). \qquad (21)$$

For each experiment carried out with an insulating lid, we can compute the length h that gives $\overline{Q(h)}$ equal to the observed heat flux. The results are plotted in Figure 16 using not directly h, but the length $h - a/2$, which we will call ℓ_c. With the model used here, given by equation (19) and Figure 15, this length ℓ_c can be seen as the critical length, after the border of the lid, for the formation of a cold downwelling. We showed that the width of the cellular circulation depends on the Rayleigh number, with a relationship scaling as $\Lambda \sim Ra^{1/4}$, and this trend is clearly visible in Figure 16. On the other hand, the length ℓ_c appears to depend poorly on Ra and on the width a of the lid, and stays broadly close to $\ell_c = 1$.

[32] The position where the first cold plume forms on each side of the lid can also be detected in each experiment using the method described in section 3.3, based on the boundary layer Rayleigh number Ra_δ. The position x of the first cold downwelling is defined so that $Ra_\delta = Ra_c$ at $x = a/2 + \ell_c$. This method was used for 100 snapshots of the heat flux distribution using $Ra_c = 50$ for experiments with $10^5 < Ra < 5.10^7$ and $0.5 < a < 4$, and the results are presented in Figure 17. We obtained a mean value of ℓ_c equal to 1.245 with a standard deviation of 0.482. Figure 17 also presents the results obtained for a fixed width a of the lid and for a fixed Rayleigh number. This indicates that ℓ_c seems to depend slightly on both a and Ra, with larger values of ℓ_c obtained for small Ra or large a.

[33] The mean value $\overline{\ell_c} = 1.245 \pm 0.482$ is consistent with what was obtained through the resolution of equation (21) (see Figure 16), indicating that the approach that we used to compute the mean heat flux, presented in Figure 15, is

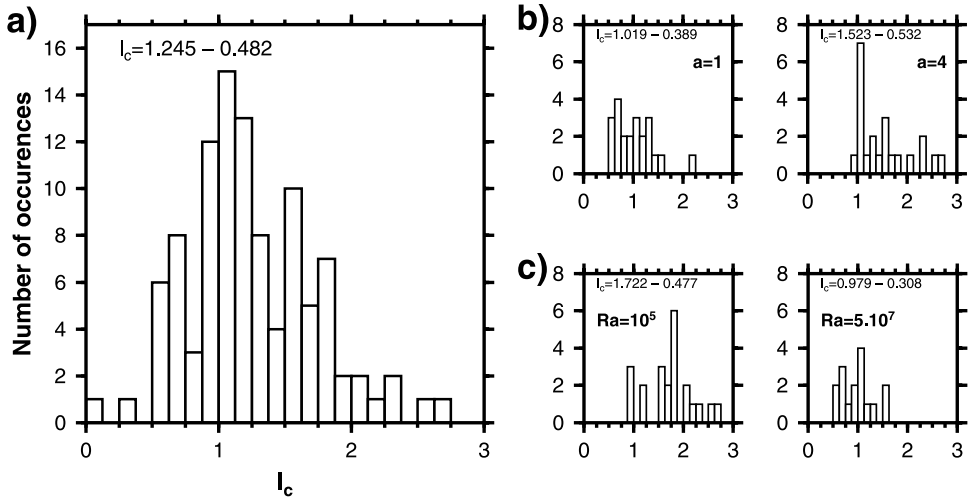

Figure 17. Histograms of the observed length ℓ_c, for 100 snapshots in experiments carried out under a perfectly insulating lid with various lid width a and Rayleigh numbers Ra. (a) Results for all the experiments. (b) Results limited to $a = 1$ and $a = 4$ and (c) to $Ra = 10^5$ and $Ra = 5.10^7$. The mean and standard deviation are indicated on top of each case.

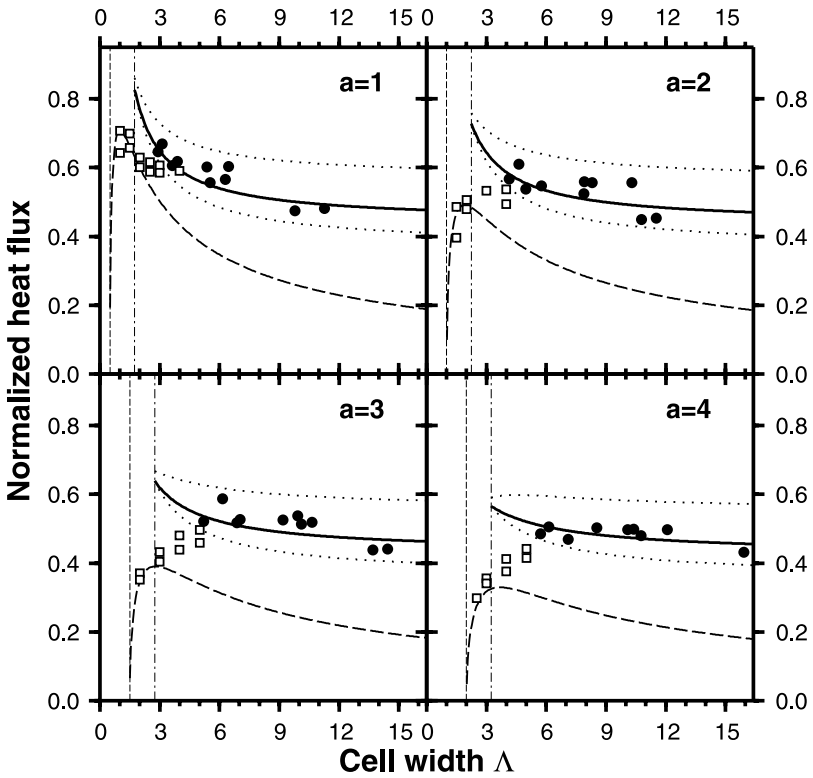

Figure 18. Observed and predicted heat flux normalized on the heat flux obtained for a cell of width 1 in simple Rayleigh-Bénard convection, as a function of the size of the cellular circulation generated by the lid, for different widths a of the lid. The solid circles are obtained in models of aspect ratio 32, while the open squares are obtained in models of limited aspect ratios, up to 10. Results are obtained for $10^5 < Ra < 5.10^7$. The solid line is plotted using equation (21), with $\overline{\ell_c} = 1.245$, while the dashed line corresponds to equation (18). The two dotted lines correspond to $\overline{\ell_c} \pm 0.482$. The vertical dashed lines indicate the limit of possible models for equation (18) ($\Lambda > a/2$), and the vertical dot-dashed lines indicate the limit of possible models for equation (21) ($\Lambda > \ell_c + a/2$).

validated by the observation of the positions of the cold plumes.

[34] The observed mean heat flux over the cellular circulation of width Λ generated by the lid is plotted in Figure 18. We also indicate some results for boxes of smaller aspect ratios, and these results can be compared to the scaling laws given by equation (18) from *Grigné et al.* [2007], which are valid for models of aspect ratio up to 4, that is to say cells of width up to 2 (dashed line), and to the scaling law given by equation (21) derived above (solid line). The discrepancy between the obtained heat flux and the model given by equation (18) is clear for cells of width larger than 2, and the heat flux for cells of moderate sizes seem to undergo a transition toward the model proposed here for large aspect ratio models (equation (21)). This latter model fits nicely the results obtained in models of aspect ratio 32.

5. Discussion and Implications for Terrestrial Planets

[35] The presence of a lid of finite conductivity on top of an isoviscous fluid heated from the bottom generates a special pattern of convection, with one hot upwelling or a set of hot plumes present beneath the lid, and large cellular circulations on both sides of the lid. In experiments carried out in boxes of small aspect ratios [*Grigné et al.*, 2007], we identified two regimes of convection, distinguishable by the fact that the hot upwelling beneath the lid consists of one single feature (forced loop) or of a set of small plumes (free loop). In both regimes, the zone of cold downwelling stays narrow and its position is imposed by the geometry of the model. In the present paper, we used very wide models in order to let this zone of cold downwelling adopt a free behavior, and we obtained broad zones of downwellings with small cold plumes forming at a certain distance from the edge of the lid and being pushed away from the lid. We showed that the distance ℓ_c at which the cold plumes start forming was fairly independent of Ra and of the width a of the lid, and is close to 1.25.

[36] We showed that the width Λ of the cellular circulation generated by the lid scales to first order as $\Lambda \sim Ra^{1/4}$. This large horizontal circulation cannot be treated as simple convective cells, and the scaling for the heat flux that we built for small aspect ratio boxes, based on a loop model approach [*Grigné et al.*, 2007], does not apply for wide box experiments. We proposed here a new scaling for these cases, in which we separate the large cellular circulation generated by the lid into two parts, one close to the lid where a half-space cooling model can apply, and a second zone starting where the first cold plumes appear in the upper boundary layer, and for which the heat flux is broadly

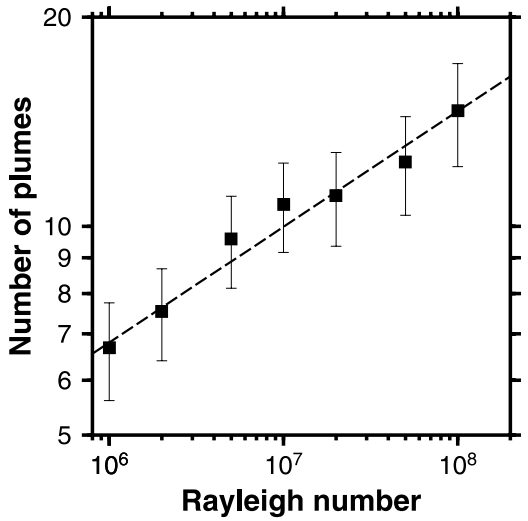

Figure 19. Time-averaged number of hot plumes N_p detected in two-dimensional models of aspect ratios 32, with a continental lid of width $a = 1$ and Biot number $B = 10$. The detection of plumes is done over the region between $x = 13$ and $x = 19$, with the continent center located at $x = 16$. The dashed line is drawn using $N_p = 0.680\ Ra^{1/6}$. The error bars correspond to the standard deviation between the time-averaged value of N_p and instantaneous values.

uniform. The fact that the cold boundary layer does not keep thickening far from the lid, but is mobilized by the formation of cold plumes, implies that the mean heat flux does not decrease with the width Λ of the cellular circulation, which would be predicted with a simple convective cell in a loop model, but is to first-order independent of Λ for $\Lambda > 3$.

[37] The observation that the oceanic heat flux is broadly uniform for seafloor older than 80 Myr has been attributed to the onset of small-scale convection under the lithosphere [*Parsons and McKenzie*, 1978; *Davaille and Jaupart*, 1994; *Doin and Fleitout*, 2000; *Dumoulin et al.*, 2001; *van Hunen et al.*, 2003] which is well understood when computing the Rayleigh number of a boundary layer thickening with time [*Howard*, 1964]. The same physics applies here except that the whole boundary layer is destabilized, instead of the small low-viscosity sublayer in the more realistic temperature-dependent viscosity case [*Davaille and Jaupart*, 1994]. The scaling for the total surface heat flow has to account for this destabilization since the heat flux in the unstable region is significantly larger than the still decreasing extrapolation of the half-space cooling expression. The situation is different on Earth where the correction from the small-scale convection is small [*Jaupart et al.*, 2007] because again only a small part of the boundary layer is destabilized. This points to the two main missing ingredients of the present model: temperature dependence of the viscosity and a failure mechanism to go from stagnant lid convection to plate tectonics [e.g., *Bercovici*, 1998; *Tackley*, 2000b].

[38] The main effect of the destabilization of the boundary layer is to limit the possible decrease of heat flux with age of the seafloor. In the present isoviscous model this effect is dramatic and this implies a rather small influence on the global heat transfer characteristics. On Earth, only a small sublayer is mobilized by these instabilities and only a small enhancement of the heat flux is observed compared to the case of a half-space cooling model for the whole lithosphere [*Jaupart et al.*, 2007]. In this case, if continents play the same role of increasing the wavelength of convection as they do in isoviscous models, and there is no reason why they would not, we expect a strong decrease of heat transfer by mantle convection compared to a situation without continents.

[39] Our models show the presence of a set of hot plumes beneath the continental lid. It was proposed by *Schubert et al.* [2004] that what is often described as superplumes could be smaller structures not revealed by seismic resolution, and that the so-called "superplumes" under the Pacific Ocean and Africa could, in fact, be plume clusters. Although there are evidences of a compositional origin for the hot upwelling observed under Africa [*Ishii and Tromp*, 1999; *Masters et al.*, 2000; *Ni et al.*, 2002; *Trampert et al.*, 2004; *McNamara and Zhong*, 2005], and although our models account only for thermal convection, with no chemical heterogeneities, it can be pointed out that the pattern of convection consisting of a cluster of plumes appears naturally in experiments where a part of the surface is thermally insulating, and that it can be inferred that the presence of the African continent may easily enhance the formation of hot plumes.

[40] The number of plumes in such a plume cluster, from our two-dimensional experiments, seems to increase with the Rayleigh number (see Figure 3). Detecting plumes at the base of the model with the method described in section 3.3, using the boundary layer Rayleigh number (see equation (17) and Figure 13), allows us to obtain a scaling for the number of plumes observed under the continental lid as a function of the Rayleigh number. Plume detection is carried out for $10^6 \leq Ra \leq 10^8$ in models of aspect ratio 32 with a lid of width $a = 1$ located at $x = 16$ and we sum the number of plumes detected over the region $13 \leq x \leq 19$. This width corresponds broadly to the width of the continental cells at $Ra = 10^6$ (see Figures 3 and 5) and thus allows to compare the number N_p of plumes detected at different Rayleigh numbers over a region where the dominant dynamics is the attraction of hot plumes toward the center of the lid. Figure 19 shows that we obtain a time-averaged number of plumes N_p so that $N_p \sim Ra^{1/6}$. *Zhong* [2005] showed that in two-dimensional models the number of plumes scales as $N_p \sim Ra^n$, where $n = 2\beta - \nu$, with β corresponding to the scaling for the heat flux ($Q \sim Ra^{\beta}$) and ν corresponding to the scaling for the horizontal velocity ($U \sim Ra^{\nu}$). For classical Rayleigh-Bénard convection, $\beta = 1/3$ and $\nu = 2/3$, so that $n = 0$, and N_p does not depend on Ra, meaning that the dominant horizontal scale is broadly constant with Ra and close to the depth of the domain. With a continental lid, we obtain a heat flux still scaling as $Ra^{1/3}$ (equation (21)), but we showed that the horizontal velocity scales as $U \sim Ra^{1/2}$ (see Figure 10), thus implying $n = 2/3 - 1/2 = 1/6$. Figure 19 shows that we observe this scaling $N_p \sim Ra^{1/6}$.

[41] We so far presented only two-dimensional experiments. A few three-dimensional experiments were also carried out, and an example is shown in Figure 20: The pattern of convection is quite similar to the one obtained in two-dimensional experiments, with clearly a set of small hot plumes under the lid, and cold plumes forming in the upper

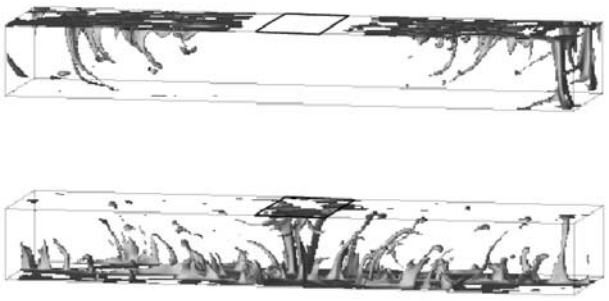

Figure 20. Isotherms (top) $T = 0.3$ and (bottom) $T = 0.7$ obtained for $Ra = 10^7$ in a Cartesian three-dimensional model, of aspect ratio 8×2, with a perfectly insulating lid. The limits of the lid are indicated with gray lines.

boundary layer away from the lid. It can also be noted that the hot plumes attracted under the lid, as is observed in the two-dimensional experiments, are bent by the large-scale circulation generated by the lid, so that their traces at the surface would be on the edge of the continents. This bending can be proposed to explain the positions of some hot spots around Africa, as an alternative to the model of edge-driven small-scale convection proposed by *King and Anderson* [1998] and *King and Ritsema* [2000].

[42] A large horizontal circulation is obtained in the models, showing that a narrow continental lid can have a broad effect on mantle flow. This effect is enhanced at high Rayleigh number, and we showed that the width of the flow affected by the presence of the lid scales as $Ra^{1/4}$. This feature can have important effects on the formation of heterogeneities at the surface of a terrestrial planet. The surface of Mars presents a clear dichotomy between highlands in the southern hemisphere and lowlands in the northern hemisphere. The origin of this dichotomy can be either exogenic (impact) or endogenic, and in the latter case, it is usually believed that the pattern of convection inside of Mars must be of degree 1 [*Roberts and Zhong*, 2006]. Obtaining such a pattern has remained challenging and several parameters have been included in models to try to reproduce this degree 1 mantle convection, such a phase transition close to the bottom of the Martian mantle and/or a depth-dependent viscosity [e.g., *Harder and Christensen*, 1996; *Zhong and Zuber*, 2001]. The results of the present study suggest that continent-like heterogeneities at the surface of the Martian mantle can also help generating degree 1 mantle convection, especially in the early stages of the cooling of Mars when the Martian mantle was probably hotter, and thus had a lower viscosity and more vigorous convection.

[43] The implications for the Earth are also important, particularly in its early history: Models of convection trying to generate plate tectonics in a self-consistent way [e.g., *Moresi and Solomatov*, 1998; *Tackley*, 2000a; *Bercovici*, 2003] show that plate tectonics is often stable only when a long wavelength of mantle convection is attained. This long wavelength often develops slowly in models with homogeneous boundary conditions, and we infer from our results that the early presence of thermally insulating continent-like heterogeneities at the surface of the mantle can help generate a long-wavelength pattern of convection and promote the onset of plate tectonics.

[44] **Acknowledgments.** We wish to thank Associate Editor Steve Cohen and Shijie Zhong for constructive reviews. All figures have been produced using the Generic Mapping Tool of *Wessel and Smith* [1998]. This work was supported by the program "Intérieur de la Terre" of INSU and NSF grant EAR-022950. This is ETH contribution 1492.

References

Bercovici, D. (1998), Generation of plate tectonics from lithosphere-mantle flow and void-volatile self-lubrication, *Earth Planet. Sci. Lett.*, *154*, 139–151.

Bercovici, D. (2003), The generation of plate tectonics from mantle convection, *Earth Planet. Sci. Lett.*, *205*, 107–121.

Busse, F., M. A. Richards, and A. Lenardic (2006), A simple model of high Prandtl and high Rayleigh number convection bounded by thin low-viscosity layers, *Geophys. J. Int.*, *164*, 160–167.

Davaille, A., and C. Jaupart (1994), Onset of thermal convection in fluids with temperature-dependent viscosity: Application to the oceanic mantle, *J. Geophys. Res.*, *99*, 19,853–19,866.

Doin, M.-P., and L. Fleitout (2000), Flattening of the oceanic topography and geoid: Thermal versus dynamic origin, *Geophys. J. Int.*, *143*, 582–594.

Dubuffet, F., D. A. Yuen, and M. Rabinowicz (1999), Effects of a realistic mantle thermal conductivity on the pattern of 3-D convection, *Earth Planet. Sci. Lett.*, *171*, 401–409.

Dumoulin, C., M.-P. Doin, and L. Fleitout (2001), Numerical simulations of the cooling of an oceanic lithosphere above a convective mantle, *Phys. Earth Planet. Intet.*, *125*, 45–64.

Grigné, C., and S. Labrosse (2001), Effects of continents on Earth cooling: Thermal blanketing and depletion in radioactive elements, *Geophys. Res. Lett.*, *28*, 2707–2710.

Grigné, C., S. Labrosse, and P. J. Tackley (2005), Convective heat transfer as a function of wavelength: Implications for the cooling of the Earth, *J. Geophys. Res.*, *110*, B03409, doi:10.1029/2004JB003376.

Grigné, C., S. Labrosse, and P. J. Tackley (2007), Convection under a lid of finite conductivity: Heat flux scaling and application to continents, *J. Geophys. Res.*, *112*, B08402, doi:10.1029/2005JB004192.

Guillou, L., and C. Jaupart (1995), On the effect of continents on mantle convection, *J. Geophys. Res.*, *100*, 24,217–24,238.

Gurnis, M. (1988), Large-scale mantle convection and the aggregation and dispersal of supercontinents, *Nature*, *332*, 695–699.

Hager, B., R. Clayton, M. Richards, R. Corner, and A. Dziewonski (1985), Lower mantle heterogeneity, dynamic topography and the geoid, *Nature*, *313*, 541–545.

Hansen, U., and A. Ebel (1984), Experiments with a numerical-model related to mantle convection—Boundary layer behavior of small-scale and large-scale flows, *Phys. Earth Planet. Inter.*, *36*, 374–390.

Hansen, U., D. Yuen, S. Kroening, and T. Larsen (1993), Dynamic consequences of depth-dependent thermal expansivity and viscosity on mantle circulations and thermal structure, *Phys. Earth Planet. Inter.*, *77*, 205–223.

Harder, H., and U. R. Christensen (1996), A one-plume model for martian mantle convection, *Nature*, *308*, 507–509.

Honda, S., M. Yoshida, S. Ootorii, and Y. Iwase (2000), The timescales of plume generation caused by continental aggregation, *Earth Planet. Sci. Lett.*, *176*, 31–43.

Howard, L. N. (1964), Convection at high Rayleigh number, in *Proceedings of the Eleventh International Congress of Applied Mechanics*, edited by H. Gortler, pp. 1109–1115, Springler-Verlag, New York.

Ishii, M., and J. Tromp (1999), Normal-mode and free-air gravity constraints on lateral variations in velocity and density of Earth's mantle, *Science*, *285*, 1231–1236.

Jaupart, C., and J. Mareschal (1999), The thermal structure and thickness of continental roots, *Lithos*, *48*, 93–114.

Jaupart, C., S. Labrosse, and J.-C. Mareschal (2007), Temperatures, heat and energy in the mantle of the Earth, in *Treatise of Geophysics, Mantle Dynamics*, vol. 7, Elsevier, New York, in press.

King, S. D., and D. L. Anderson (1998), Edge-driven convection, *Earth Planet. Sci. Lett*, *160*, 289–296.

King, S. D., and J. Ritsema (2000), African hot spot volcanism; small-scale convection in the upper mantle beneath cratons, *Science*, *290*, 1137–1140.

Koschmieder, E. L. (1993), *Bénard Cells and Taylor Vortices*, Cambridge Univ. Press, Cambridge, U.K.

Krishnamurti, R., and L. N. Howard (1981), Large-scale flow generation in turbulent convection, *Proc. Natl. Acad. Sci. U.S.A.*, *78*(4), 1981–1985.

Lenardic, A., and L. Moresi (2001), Heat flow scaling for mantle convection below a conducting lid: Resolving seemingly inconsistent modeling results regarding continental heat flow, *Geophys. Res. Lett.*, *28*, 1311–1314.

Masters, G., G. Laske, H. Bolton, and A. M. Dziewonski (2000), The relative behavior of shear velocity, bulk sound speed, and compressional velocity in the mantle: Implications for chemical and thermal structure, in *Earth's Deep Interior: Mineral Physics and Tomography From the Atomic to the Global Scale*, *Geophys. Monogr. Ser.*, vol. 117, edited by S. Karato et al., pp. 66–87, AGU, Washington, D. C.

McNamara, A., and S. Zhong (2005), Thermochemical structures beneath Africa and the Pacific Ocean, *Nature*, *437*, 1136–1139.

Michaut, C., and C. Jaupart (2004), Nonequilibrium temperatures and cooling rates in thick continental lithosphere, *Geophys. Res. Lett.*, *31*, L24602, doi:10.1029/2004GL021092.

Montagner, J.-P. (1994), Can seismology tell us anything about convection in the mantle?, *Rev. Geophys.*, *32*, 115–138.

Moresi, L., and V. Solomatov (1998), Mantle convection with brittle lithosphere: thoughts on the global tectonic styles of the Earth and Venus, *Geophys. J. Int.*, *133*, 669–682.

Ni, S., E. Tan, M. Gurnis, and D. Helmberger (2002), Sharp sides to the African superplumes, *Science*, *296*, 1850–1852.

Olson, P., and G. Corcos (1980), A boundary-layer model for mantle convection with surface plates, *Geophys. J. R. Astron. Soc.*, *62*, 195–219.

Parsons, B., and D. P. McKenzie (1978), Mantle convection and the thermal structure of the plates, *J. Geophys. Res.*, *83*, 4485–4496.

Phillips, B. R., and H.-P. Bunge (2005), Heterogeneity and time dependence in 3d spherical mantle convection models with continental drift, *Earth Planet. Sci. Lett.*, *233*, 121–135.

Roberts, J. H., and S. Zhong (2006), Degree-1 convection in the Martian mantle and the origin of the hemispheric dichotomy, *J. Geophys. Res.*, *111*, E06013, doi:10.1029/2005JE002668.

Rudnick, R., W. McDonough, and R. O'Connell (1998), Thermal structure, thickness and composition of continental lithosphere, *Chem. Geol.*, *145*, 395–411.

Schubert, G., G. Masters, P. Olson, and P. J. Tackley (2004), Superplumes or plume clusters, *Phys. Earth Planet. Inter.*, *146*, 147–162.

Sotin, C., and S. Labrosse (1999), Three-dimensionnal thermal convection of an isoviscous, infinite–Prandtl–number fluid heated from within and from below: Applications to heat transfer in planetary mantles, *Phys. Earth Planet. Inter.*, *112*, 171–190.

Sparrow, E., R. Goldstein, and V. Jonsson (1964), Thermal instability in a horizontal layer: Effect of boundary conditions and non-linear temperature profile, *J. Fluid. Mech.*, *18*, 513–528.

Su, W.-J., and A. Dziewonski (1991), Predominance of long-wavelength heterogeneity in the mantle, *Nature*, *352*, 121–126.

Tackley, P. J. (1993), Effects of strongly temperature-dependent viscosity on time-dependent, three-dimensional models of mantle convection, *Geophys. Res. Lett.*, *20*, 2187–2190.

Tackley, P. J. (1996), Effects of strongly variable viscosity on three-dimensional compressible convection in planetary mantles, *J. Geophys. Res.*, *101*, 3311–3332.

Tackley, P. J. (2000a), Self-consistent generation of tectonic plates in time-dependent, three-dimensional mantle convection simulations, *Geochem. Geophys. Geosyst.*, *1*(8), doi:10.1029/2000GC000036.

Tackley, P. J. (2000b), Mantle convection and plate tectonics; towards an integrated physical and chemical theory, *Science*, *288*, 2002–2007.

Trampert, J., F. Deschamps, J. Resovsky, and D. Yuen (2004), Probalistic tomography maps chemical heterogeneities throughout the lower mantle, *Science*, *306*, 853–856.

Turcotte, D., and G. Schubert (1982), *Geodynamics: Application of Continuum Physics to Geological Problems*, John Wiley, New York.

Turcotte, D., and G. Schubert (2002), *Geodynamics*, Cambridge Univ. Press, New York.

van Hunen, J., J. Huang, and S. Zhong (2003), The effect of shearing on the onset and vigor of small-scale convection in a Newtonian rheology, *Geophys. Res. Lett.*, *30*(19), 1991, doi:10.1029/2003GL018101.

Wessel, P., and W. H. F. Smith (1998), New, improved version of Generic Mapping Tools released, *Eos Trans. AGU*, *79*(47), 579.

Woodward, R. L., and G. Masters (1991), Lower-mantle structure from ScS-S differential travel times, *Nature*, *352*, 231–233.

Yoshida, M., Y. Iwase, and S. Honda (1999), Generation of plumes under a localized high viscosity lid in 3D spherical shell convection, *Geophys. Res. Lett.*, *26*, 947–950.

Zhang, Y.-S., and T. Tanimoto (1991), Global Love wave phase velocity variation and its significance to plate tectonics, *Phys. Earth Planet. Inter.*, *66*, 160–202.

Zhong, S. (2005), Dynamics of thermal plumes in three-dimensional isoviscous thermal convection, *Geophys. J. Int.*, *162*, 289–300.

Zhong, S., and M. Gurnis (1993), Dynamic feedback between a continent like raft and thermal convection, *J. Geophys. Res.*, *98*, 12,219–12,232.

Zhong, S., and M. T. Zuber (2001), Degree-1 mantle convection and the crustal dichotomy on Mars, *Earth Planet. Sci. Lett.*, *189*, 75–84.

C. Grigné and P. J. Tackley, Institut für Geophysik, ETH Zürich, ETH Hönggerberg HPP, Zürich CH-8093, Switzerland. (cecile.grigne@erdw.ethz.ch; ptackley@ethz.ch)

S. Labrosse, Sciences de la Terre, Ecole Normale Supérieure de Lyon, 46 Allée d'Italie, F-69364 Lyon Cedex 07, France. (stephane.labrosse@ens-lyon.fr)